Biophysical Journal Volume 81 August 2001 1047–1058

Rational Design of Lipid Molecular Structure: A Case Study Involving the C19:1c10 Monoacylglycerol

Y. Misquitta* and M. Caffrey*†

*Biophysics, †Biochemistry, and †Chemistry, The Ohio State University, Columbus, Ohio 43210 USA

ABSTRACT The phase properties of lipids have far-reaching consequences in membrane biology. Their influence ranges from domain formation in intact biomembranes to membrane protein reconstitution and crystallization. To exploit phase behavior in the spirit of rational design, it is imperative that the rules relating lipid molecular structure and liquid crystal or mesophase behavior be established. Phase behavior is quantitatively and concisely represented in the form of temperature-composition phase diagrams. A somewhat limited number of phase diagrams exists for the monoacylglycerols. The objective of the current study was to determine the quality of phase behavior prediction for a specific monoacylglycerol based on an analysis of the existing phase diagrams for related chain homologs. To this end, a phase diagram for the monononadecenoin (19:1c10)/water system was predicted in the temperature range from −15°C to 120°C and from 0% to 80% (w/w) water. The prediction was tested by constructing the corresponding phase diagram using low- and wide-angle x-ray diffraction, differential scanning calorimetry, and polarized light microscopy. The results show that the predicted and experimental phase diagrams agree remarkably well. They also highlight the need for additional phase studies of the type described to enlarge the data bank of phase diagrams and to strengthen the foundations of the rational design approach.

INTRODUCTION

A considerable amount is known about the phase properties of lipids. This knowledge has accumulated in response primarily to a need to understand the role played by the lipid component of biological membranes. Increasingly, the physical properties of lipids and in particular their propensity for forming different liquid crystal or mesophases, are being recognized as impacting on membrane function. The recent flurry of activity in the area of rafts (Brown and London, 1998, 2000; Simons and Ikonen, 2000) is just one example of where lipids are clearly implicated in modulating membrane function.

There are other areas where lipid phase properties have become the focus of much attention. These include controlled drug release (Jones and Chapman, 1995; Engström, 1990) and nucleic acid delivery (Boulikas, 1996; Lasic, 1997). Membrane protein crystallization, and thus structure determination, has also benefited from lipid phase studies with the advent of a new approach for growing diffraction-quality crystals in a lipidic cubic mesophase (Landau et al., 1997, Luecke et al., 1998). Despite the success and potential import of the method, we know essentially nothing of how crystals grow in such an environment or indeed the role of the mesophase in the process. This represents a very active area of research currently (Caffrey, 2000).

The biological membrane, and indeed the aforementioned lipidic incubus in which membrane protein crystals develop, are complex systems. The complexity is associated, at least in part, with the myriad of components they contain, how each impacts on the system's collective phase behavior, and how these effects are modified by the bathing aqueous medium and the physical environment. With a view to understanding, and thus exploiting, these assorted effects, we have chosen the reductionist approach. This involves working with relatively simple systems consisting of a single lipid species and water. While having few components, the model system still expresses the phase behavior of interest, but more importantly it can be manipulated in controlled ways so as to trigger a measurable response in mesomorphism.

One of the goals of our work is to decipher the rules concerning the manner in which mesomorphism is determined by lipid molecular structure. We have chosen to examine this issue using monoacylglycerols as the test lipid because of their structural simplicity and ready availability. They also exhibit a very rich mesomorphism when dispersed with water at moderate temperatures. It is also worthwhile noting that the monoacylglycerol monoolein (18:1c9) was used in the development and implementation of the *in meso* method for membrane protein crystallization.

We have invested considerable effort in characterizing the lyotropic (water-dependent) and thermotropic (temperature-dependent) phase properties of the monoacylglycerols, with an emphasis on those containing a long, *cis* monounsaturated acyl chain. In the course of this work, we have mapped out temperature-composition phase diagrams for several monoacylglycerol chain homologs (Briggs, 1994;

Received for publication 12 February 2001 and in final form 1 May 2001.

Address reprint requests to Dr. Martin Caffrey, The Ohio State University, Biochemistry, Biophysics, Chemistry, 100 W 18th Avenue, Columbus, OH 43210. Tel.: 614-292-8437; Fax: 614-292-1532; E-mail: caffrey.1@osu.edu

Abbreviations used: DSC, differential scanning calorimetry; FI, fluid isotropic phase; H_{II}, inverted hexagonal phase; Lα, lamellar liquid crystal phase; Lc, lamellar crystal phase; MEc, monoeicosenoin (20:1c11); MEr, monoerucin (22:1c13); MHt, monoheptadecenoin (17:1c10); MNd, monononadecenoin (19:1c10); MOl, monoolein (18:1c9); MPt, monopentadecenoin (15:1c10); PLM, polarized light microscopy; TRXRD, time-resolved x-ray diffraction.

0006-3495/01/08/1047/12 $2.00

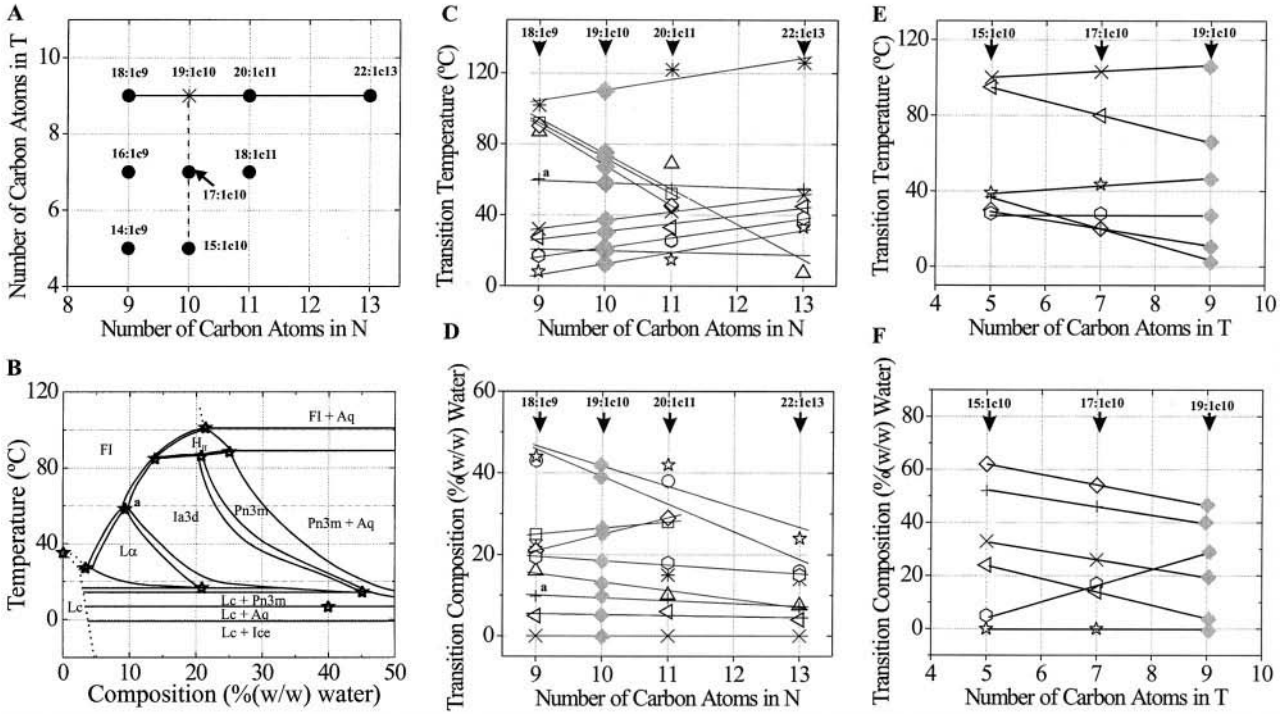

FIGURE 1 (*A*) Location in *N-T* space of the monoacylglycerols discussed in this study. The asterisk shows the position of MNd (19:1c10), the subject of the current work. (*B*) The phase transition temperatures and compositions obtained from the monoolein/water phase diagram (redrawn from Qiu and Caffrey, 2000) that are used in *C–F* are identified by a star (☆). Thus, the Lα-to-(Ia3d+FI) transition identified by a superscript *a* occurs at ~60°C and 10% (w/w) water. These data are similarly marked with a superscript *a* in *C* and *D*. (*C* and *D*) Phase transition temperature (*C*) and phase transition composition (*D*) as a function of *N*, the number of carbon atoms in the neck portion of the monoacylglycerol acyl chain. The homologous series represented in this plot has *T*, the number of carbon atoms in the tail portion of the monoacylglycerol acyl chain, at a constant value of 9. The identity of the individual transitions and the monoacylglycerols are as follows: ☆, Lc-to-liq. cryst. (this refers to the lowest temperature at which any of the liquid crystalline (liq. cryst.) phases appears); ○, (Lc+Ia3d)-to-(Lα+Ia3d); ○, (Lc+Pn3m)-to-(Ia3d+Pn3m); ◁, Lc-to-(Lα+FI); ×, dry lipid melting; +, (Lα+FI)-to-(Ia3d+FI); △, (Ia3d+FI)-to-(Pn3m+H_{II}); ◇, (Ia3d+FI)-to-(H_{II}+FI); □, Pn3m-to-H_{II}; ✳, H_{II}-to-FI. The solid lines represent lines of best fit. The predicted transition temperatures and compositions for the MNd system were obtained by interpolation and are indicated by the filled diamond symbols. These were used in constructing the predicted phase diagram shown in Fig. 3. (*E* and *F*) Phase transition temperature (*E*) and phase transition composition (*F*) as a function of *T*. The homologous series represented in this plot has *N* at a constant value of 10. The identity of the individual transitions and the monoacylglycerols are as follows: ○, dry lipid melting; ◇, Lc-to-(Lα+FI); +, (Lα+FI)-to-(Ia3d+FI); ☆, (lamellar+Pn3m)-to-(Ia3d+Pn3m); ◁, (lamellar+Aq)-to-(Pn3m+Aq); ×, (Pn3m+Aq)-to-(FI+Aq). The predicted transition temperatures and compositions for the MNd system were obtained by extrapolation and are indicated by the filled diamond symbols. Other conditions are as outlined above.

Briggs and Caffrey, 1994a,b; Briggs et al., 1996; Chung and Caffrey, 1995; Qiu, 1998; Qiu and Caffrey, 1998, 1999, 2000). Our long-term objective is to use this information in establishing rules for the rational design of lipids having desired phase properties. Accordingly, we decided to put our existing, but somewhat limited, knowledge base to the test to see how good predictions based upon it might be. We chose the monoacylglycerol monononadecenoin (MNd, 19:1c10) as the target lipid and set about predicting its temperature-composition phase diagram when dispersed with water. The goodness, or otherwise, of the prediction was tested by comparing it with the experimental phase diagram.

By way of explaining how the predicted phase diagram was arrived at, we begin by introducing what has proven for us to be a useful way for considering how the different monoacylglycerol homologs are related. This takes the form of what is called the *N-T* matrix (Fig. 1 *A*). Here, a given lipid is assigned a coordinate in *N-T* space as dictated by the length of the chain on either side of the olefinic bond. The region between the double bond and the glycerol headgroup is referred to as the neck, denoted *N*, whereas the tail, *T*, represents that region of the chain extending from the double bond to the methyl terminus. *N* and *T* have values representing the number of carbon atoms in the respective regions of the chain (Fig. 2).

The focus of this work, MNd (19:1c10), has a fatty acyl chain 19 carbon atoms long with a single *cis* double bond at carbon number 10 (Fig. 2). In the *N-T* notation, it is represented by $N = 10$ and $T = 9$ (asterisk in Fig. 1 *A*). Also included in Fig. 1 *A* is a series of monoacylglycerols for which detailed phase diagrams are available. One series includes monoolein (MOl, 18:1c9), monoeicosenoin (MEc, 20:1c11), and monoeruccin (MEr, 22:1c13). These represent *N* homologs of MNd where *N* varies from 9 to 13, while

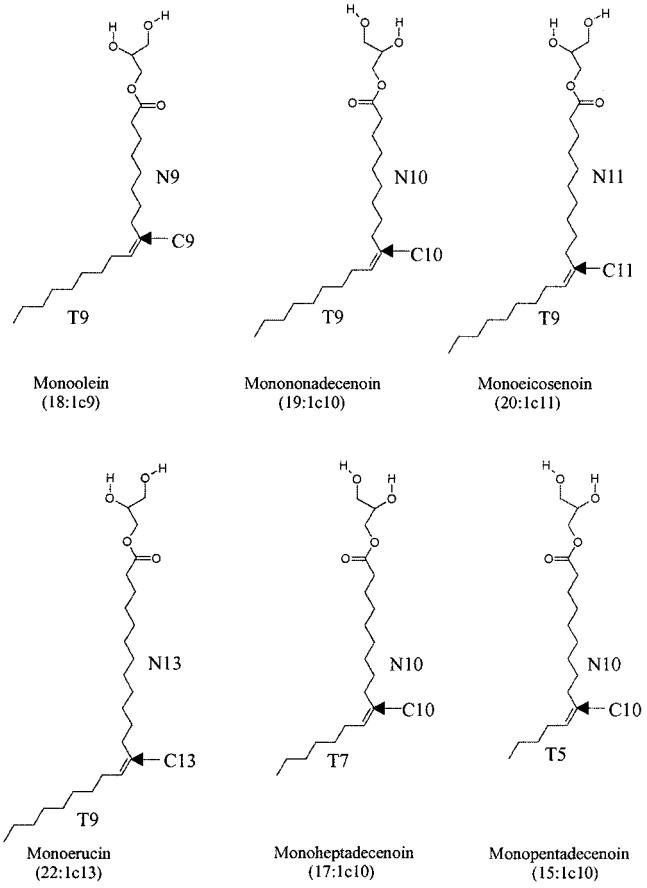

FIGURE 2 The molecular structures of the monoacylglycerols in the homologous series examined in this study. The common and shorthand names of the monoacylglycerols are shown. All of the monoacylglycerols have *cis* double bonds at the indicated positions along the chain. The length of the neck (*N*) and tail (*T*) portions of the acyl chain is also shown.

T remains constant at a value of 9 within the series (solid line in Fig. 1 *A*). The second homologous series has *N* fixed at a value of 10 while *T* varies from 5 (monopentadecenoin, MPt, 15:1c10) to 7 (monoheptadecenoin, MHt, 17:1c10) (dashed line in Fig. 1 *A*).

A phase diagram is represented by a series of interconnected phase fields located in temperature-composition space. A phase field represents an area in a phase diagram that is occupied by a single phase or multiple phases. Transitions between phases occur at well-defined temperatures and compositions. For each member of the homologous series represented in Fig. 1 *A*, the transition temperatures and compositions at the two- or three- phase coexistence regions have been extracted from their respective phase diagrams. An example of how these transition values were obtained in the case of the monoolein/water system is shown in Fig. 1 *B*. The transition temperatures have been plotted in Fig. 1, *C* and *E*, as a function of *N* and *T*, respectively. Assuming that transition temperatures are linearly related to *N* or *T* in the immediate vicinity of the

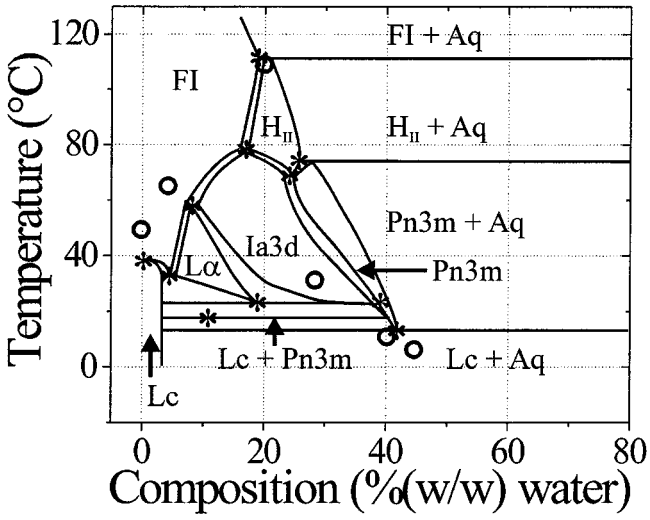

FIGURE 3 The predicted temperature-composition phase diagram for the MNd (19:1c10)/water system, based on transition temperatures and compositions expected by comparison with similar data for homologous monoacylglycerols. Predictions based on the transition temperatures from Fig. 1, *C* and *D*, and compositions from Fig. 1, *E* and *F*, are marked with asterisks and circles, respectively.

target lipid MNd, the temperature expected for the various transitions undergone by MNd were obtained by interpolation (Fig. 1 *C*) or extrapolation (Fig. 1 *E*). A similar approach was taken for the major lyotropic transitions (Fig. 1, *D* and *F*). The predicted transition temperatures and compositions were placed in a blank temperature-composition phase diagram (asterisks and circles in Fig. 3) and were used to construct a predicted phase diagram in accordance with the Gibbs phase rule and with established phase diagrams for other members of the homologous series (Briggs, 1994; Briggs and Caffrey, 1994a,b; Briggs et al., 1996; Qiu, 1998; Qiu and Caffrey, 1998, 1999, 2000). In drawing the predicted phase diagram, more weight was given to the data from Fig. 1, *C* and *D* (asterisks in Fig. 3) than to data from Fig. 1, *E* and *F* (circles in Fig. 3), because the former are based on lines of best fit defined by three data points (in all but one transition) as opposed to just two data points in the case of the latter.

By way of testing the prediction, we have constructed the equilibrium phase diagram for the MNd/water system. Phases were identified by static low- and wide-angle x-ray diffraction and by polarized light microscopy. Measurements were made in the temperature range from −15°C to 120°C (in increments of 5°C or less) and in the composition range from 0% to 74% (w/w) water (generally, in increments of 5% (w/w) water or less, except in the region above 35% (w/w) water, which represents the excess water region). Certain transition temperatures were more accurately determined by means of time-resolved x-ray diffraction (TRXRD) and differential scanning calorimetry (DSC). The phases observed include the lamellar crystal (Lc) phase, the

lamellar liquid crystal (Lα) phase, the inverted cubic (space groups Ia3d (Q230) and Pn3m (Q224)) phase, the inverted hexagonal (H_{II}) phase, and the fluid isotropic (FI) phase along with areas of coexistence with ice or water. The predicted and the experimental phase diagrams are in good agreement.

Metastable or non-equilibrium behavior was observed for the cubic-Pn3m phase of the MNd/water system. This tendency of the liquid crystal phases to undercool is of significance in comparative studies of the type reported here, as well as in practical applications, as discussed.

MATERIALS AND METHODS

Materials

MNd was purchased from Nu Chek Prep (Elysian, MN, lot M-415-A20-F) with a specified purity of >99%. Lipid purity was ascertained by thin layer chromatography (TLC) (Qiu, 1998), and the lipid was used without further purification. The detection limit of the TLC method is to ~1 μg of lipid. To determine purity, 1–100 μg of MNd was chromatographed in four different solvent systems: petroleum ether/diethyl ether, 94/6 (v/v); petroleum ether/diethyl ether/acetic acid, 75/25/1 (v/v); chloroform/acetone, 96/4 (v/v); and chloroform/acetone/acetic acid/methanol, 72.5/25/0.5/2 (v/v) on Adsorbosil Plus 1 plates (Alltech, Deerfield, IL). The plates were pre-run once with a chloroform/methanol (10:1, v/v) solution. The spots were visualized by spraying the plate with 4.2 M sulfuric acid and charring it on a hotplate at ~200°C for 30 min. A Milli-Q system (Millipore Corp., Bedford, MA) consisting of a carbon filter cartridge, two ion exchange filter cartridges, and an organic removal cartridge was used to produce water with >18 Mohms cm resistivity, which was used throughout this study.

Sample preparation

Hydrated lipid samples were prepared at room temperature (between 19°C and 24°C) using a home-built syringe mixer (Cheng et al., 1998, Qiu and Caffrey, 1998) in concentrations from 0% to 74% (w/w) water and ~10–20 mg of lipid. The low-water-content samples were extremely viscous and difficult to homogenize. Accordingly, an O-ring (Buna-N, 2-mm internal diameter, 5-mm external diameter, Fournier Rubber and Supply, Columbus, OH) was inserted between the tip of the glass barrel and the steel jacket of the mixing device (Cheng et al., 1998) to facilitate non-leaky mixing at higher pressures. The samples were then loaded into quartz capillaries (Charles Supper Co., Natick, MA) or DSC cells (see below). The water content of the samples was determined gravimetrically (Cheng et al., 1998) on 2–3-mg samples (taken before and after delivery into the capillary or DSC cell) using a microbalance (R180D, Sartorius, Edgewood, NY) with an accuracy of ~0.8% (w/w) water at concentrations between 0% and 37% (w/w) water and ~2.0% (w/w) water at concentrations above 37% (w/w) water. The lower accuracy at higher hydration arises because of the tendency of the mixture to phase separate in the mixing syringe into fully hydrated mesophase and aqueous solution after homogenization. The concentration of lipid in the sample was obtained by comparing the weight of the sample before and after drying (for a minimum of 7 days) under vacuum (0.5–1 torr, house vacuum) in a phosphorous pentoxide-containing desiccator. The capillaries were flame-sealed using a butane or propane/oxygen torch (Smith Equipment, Watertown, SD) and glued with 5-min epoxy (Hardman, Belleville, NJ). Samples were stored at 4°C for a period not exceeding 2 days before being used in diffraction or DSC measurements.

Sample purity was determined by means of TLC after completing the TRXRD (70% (w/w) water, ramped from −15°C to 120°C over an 8-h period) and DSC (11–70% (w/w) water, ramped from −15°C to 120°C at 5–20°C/h, cooled back to −15°C and rerun once) experiments. Samples were found to be >99% pure based on an analysis of 100 μg of hydrated lipid. To dissolve the used lipid in chloroform for subsequent TLC analysis, the capillaries (excluding the epoxy-sealed ends) containing the hydrated samples (~10 mg) were broken in a 1.5-ml plastic microfuge tube (Eppendorf Scientific, Westbury NY, Fisher catalog item 05–402-24B). The required amount of chloroform (~100 μl) was added, and the samples were vortexed to dissolve the lipid component. From 1 to 100 μg of MNd dissolved in chloroform was examined by TLC in four different solvent systems as described above. The samples were found to contain at least 99% monoacylglycerol. Thus, no significant damage to the samples was detected by TLC.

X-ray diffraction

Nickel-filtered (0.02 mm thick) copper Kα x-rays (1.542 Å) were used to make low- and wide-angle powder diffraction measurements. The rotating anode x-ray generator (RU-300, Rigaku U.S.A., Danvers, MA) used a 0.5-mm × 10-mm tungsten filament and was operated at 40–46 kV and 200–250 mA with a 15-cm-long vacuum (0.5–1 torr) flight tube with 0.5 mil (0.013-mm)-thick Kapton (Du Pont Electronics, Wilmington, DE) windows placed between the x-ray shutter and the mirrors. The beam was focused vertically and horizontally by a pair of 6-cm × 2-cm nickel-coated glass mirrors (Charles Supper) located ~15 cm downstream of the target. It produced a focused beam measuring 1.0 mm × 0.54 mm at the detector, which was positioned ~40 cm from the mirrors. The sample-to-detector distance was 25.7 cm or 33.8 cm and was calibrated using silver behenate with a lamellar repeat (d_{100}) of 58.37 Å (Blanton et al., 1995).

The samples were mounted in a temperature-controlled beryllium holder (Briggs and Caffrey, 1994a). The temperature was accurate to ~0.2°C at temperatures between −15°C and 120°C, as determined using a thermocouple (Physitemp Instruments, Clifton, NJ, model BAT-12) placed in a quartz capillary tube in the sample holder. The latter was calibrated against an ERTCO ASTM 64C-FC thermometer, S/N 5280 (Ever Ready Thermometer Co., West Patterson, NJ). Sample temperature was found to vary by not more than 0.02°C between −15°C and 60°C over a period of 9 h, which is the duration of a typical x-ray diffraction measurement consisting of a 4-h incubation followed by a 30-min exposure for each of seven samples.

Samples that were stored at 4°C for a period never exceeding 2 days were transferred to the beryllium holder and incubated at −15°C for 3 h or more before data collection in order to access the equilibrium Lc phase (Qiu and Caffrey, 1999, 2000). They were then heated to the required temperature and incubated there for anywhere from 3 to 6 h at which point the diffraction pattern was collected using an exposure of 30–60 min per sample. The incubation time was determined on the basis of a series of relaxation experiments, described below. This cycle of adjusting temperature followed by an incubation period was repeated up to a temperature of 120°C. To minimize the risk of chemical degradation, a single sample was used typically over a 35–45°C range corresponding to an elapsed time of 63–81 h.

To determine the appropriate pre-incubation time for the sample to attain a phase of stable lattice parameter, a series of relaxation experiments were performed with samples at 25%, 40%, and 70% (w/w) water. Initially, temperature was dropped from room temperature (20°C) to −15°C, and a 30-min diffraction measurement was made immediately. This was followed by a series of 30-min diffraction measurements made every hour for up to a maximum of 8.5 h at −15°C. A similar series of diffraction measurements were made upon sample heating to 20°C, 40°C, 80°C, and 120°C. Under most conditions, the phase lattice parameter stabilized within 2.5 h of changing temperature in the range studied. Thus, the sample

pre-incubation time used for all measurements reported here was in excess of 3 h and was typically 4 h.

Data for the construction of the metastable phase diagram was recorded from 30°C in the cooling direction. This involved an initial sample preparation at room temperature followed by a 4-h pre-incubation at 30°C at which point a 30–60-min diffraction measurement was made. Diffraction patterns (30-min duration) were recorded subsequently in the cooling direction in 5°C intervals down to −15°C with a pre-incubation at each temperature of ≥4 h.

Diffraction patterns were recorded on image plates (20 cm × 25 cm, Fuji HR-IIIN, Fuji Photo Film Co., Tokyo, Japan). Exposed plates were scanned in a phosphor image scanner (Storm 840, Molecular Dynamics, Sunnyvale, CA) at 100-μm resolution. The data were analyzed for d-spacing information using the program Fit2D (A. P. Hammersley, European Synchrotron Radiation Facility, France). The program uses two-dimensional radial averaging to produce a plot of diffracted intensity versus scattering angle (I/2-Θ), that is then fit assuming a gaussian distribution about the peak center. These data were analyzed to obtain the peak centers using the program Peakfit (Version 4, SPSS, Chicago, IL) and indexed in Microsoft Excel (Microsoft Corp., Redmond, WA). The indexing was done to find the ratios of the subsequent peaks to the first observed peak; the ratios are used to identify the phases present.

TRXRD measurements were made to define certain transition temperatures more accurately. These were done using the streak detector method where the diffraction pattern is recorded continuously as a function of temperature, as described (Caffrey, 1989; Qiu and Caffrey, 2000). For this purpose, the width of a vertical slit between a pair of lead sheets placed in front of the image plate detector was adjusted to 2–3 mm. The image plate was translated at a fixed speed (0.3 mm/min) parallel to the slit (at a constant sample-to-detector distance of 36.6 cm) while the temperature of the sample was raised at a fixed rate (0.15°C/min) by a computer under Labview (National Instruments Corp., Austin, TX) control of a program written in this laboratory.

Calorimetry

DSC measurements were made using a Hart DSC-II calorimeter (CSC4100, Calorimetry Sciences Corp., North Spanish Fork, UT). Hydrated samples (10–100 mg, total weight) were incubated at −15°C for at least 4 h to access the equilibrium Lc phase and then heated consecutively to 120°C at fixed rates ranging from 5°C to 60°C/h. Transition onset (To) and completion (Tc) temperatures were determined and were corrected for scan rate effects as described (Qiu and Caffrey, 2000). The temperature reading of the calorimeter was calibrated at 0°C with Milli-Q water equivalent in mass to that used in a typical hydrated lipid sample using the melting temperature of ice (0.0°C) at 1 atm pressure (Weast and Astle, 1982) and at 133°C using the melting point of phenacetin (provided for calibration by Mettler, Toledo, OH). The scan rates employed for the calibrations were the same (5°C to 60°C/h) as those used with the samples. Enthalpy changes (ΔH) were determined using software provided by the manufacturer. Time constant corrections are automatically made by the software provided with the calorimeter when converting data to heat capacity. This also corrects for temperature differences between the sample and the temperature sensor (Qiu, 1998).

Polarized light microscopy

The mesophase behavior of the MNd/water system was studied using polarized light microscopy (PLM) in conjunction with the penetration method (Rosevear, 1968, 1954; Qiu, 1998). Accordingly, 10–20 mg of dry (as received) lipid was placed on a microscope slide with a 150-μm-thick glass coverslip acting as a spacer between the slide and an overlaying glass coverslip that covered the sample. The sample was brought to 45°C on a Multi-Blok Heater (Lab-Line Instruments, Melrose Park, IL) causing the lipid to melt and to form a wedge by capillary action between the coverslip and the slide. Milli-Q water was introduced from the open side of the wedge while the lipid was still in a liquid phase. The water diffused into the lipid forming an activity gradient within the sample. Thus, different phases formed along the length of the gradient, which in turn were identified by their characteristic birefringent textures, or absence thereof, when examined by PLM. The sample was then cooled to room temperature at which point the lipid solidified.

Samples of fixed hydration were also examined by PLM. This involved preparing the samples in the usual way with the mixing device as described above and injecting the hydrated sample onto a glass slide. The samples were then immediately covered with a coverslip whose edges were coated with vacuum grease (HiVac-G, Shin-Etsu Chemical Co., Tokyo, Japan) to hermetically seal the sample. Care was taken to ensure the grease and lipid did not come into contact. The slide was then placed on a heating stage (FP-84 DSC-heating stage, Mettler) at room temperature and observed under the microscope (Olympus POS, McCrone Accessories and Components, Westmont, IL) at 200× and 800× magnifications. The sample was heated at a rate of 5°C/h to a temperature of 80°C. In-sample temperature was measured by a thermocouple (0.35-mm diameter, Physitemp Instruments, Clifton, NJ, model BAT-12) placed in the hydrated lipid beneath the coverslip and just out of the viewing area. Optical textures were recorded using a digital camera (Panasonic GP-KR222, Matsushita Communication Industrial Co., Tokyo, Japan) attached to the microscope, and the images were captured using the frame grabber Meteor (Matrox Electronic Systems, Dorval, Canada).

RESULTS

The primary objective of this study was to construct the equilibrium temperature-composition phase diagram of the MNd/water system and to compare it with a phase diagram predicted on the basis of similar measurements made with acyl chain homologs of MNd. A second objective was to construct the corresponding phase diagram under conditions where undercooling of the liquid crystal phases is allowed.

Equilibrium phase diagram

Given the natural inclination of lipid/water phases to undercool (Qiu and Caffrey, 2000) we sought to obviate the possible non-equilibrium behavior by collecting data in the heating direction. The issue of superheating was not examined in this study. The phase diagram in Fig. 4 was constructed in the heating direction. Samples were initially incubated at −15°C for at least 4 h to access the equilibrium solid or Lc phase. The 4-h pre-incubation time was determined as appropriate from separate relaxation measurements that established the time required for the system to acquire a stable lattice parameter (Fig. 5). Phases were identified and structurally characterized using low- and wide-angle x-ray diffraction. In the case of the Lα phase, the diffraction pattern revealed a single low-angle ring, which of course cannot be indexed. In this case, we resorted to PLM and to the mesomorphism of MNd homologs to assist in the identification of the phase, as described below. Most of the diffraction measurements were made at discrete points in temperature-composition space. These are identified in Fig. 4 as

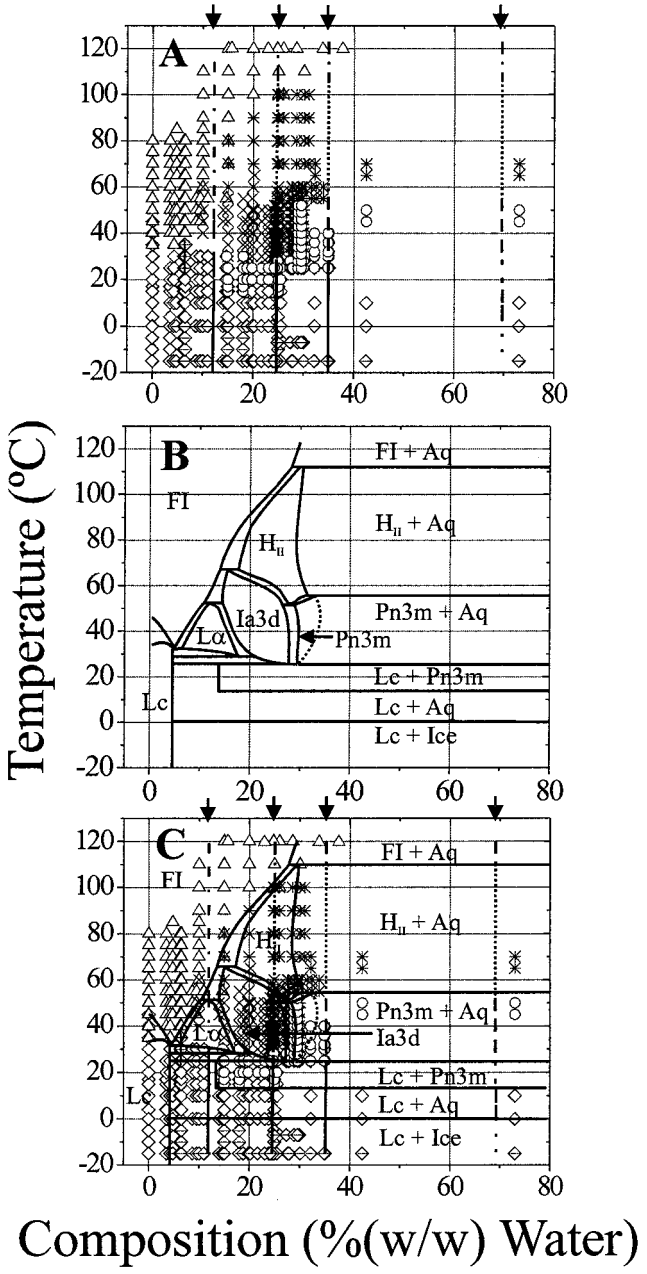

FIGURE 4 (*A*) The identity of the various phases present in the MNd/water system and their location in temperature-composition space, determined by x-ray diffraction in the heating direction. The identity of each of the phases is as follows: ◇, Lc; +, Lα; −, ice; ×, cubic-Ia3d; ○, cubic-Pn3m; △, FI; ✳, H_{II}. (*B*) Interpreted phase boundaries based on the data in *A*, on polarized light microscopy and on differential scanning calorimetric data. (*C*) An overlay of the data in *A* with the boundaries in *B*. The vertical lines in *A* and *C* (marked with *arrows*) represent calorimetric data at 11%, 24%, and 35% (w/w) water and a combination of calorimetry and TRXRD data at 70% (w/w) water. Phase type is identified along these lines as follows: · · ·, Lc+Ice; − − −, Lc+Aq; - - -, Lc+Pn3m; − − −, Pn3m+Aq; ·····, H_{II}+Aq; · - ·, FI+Aq.

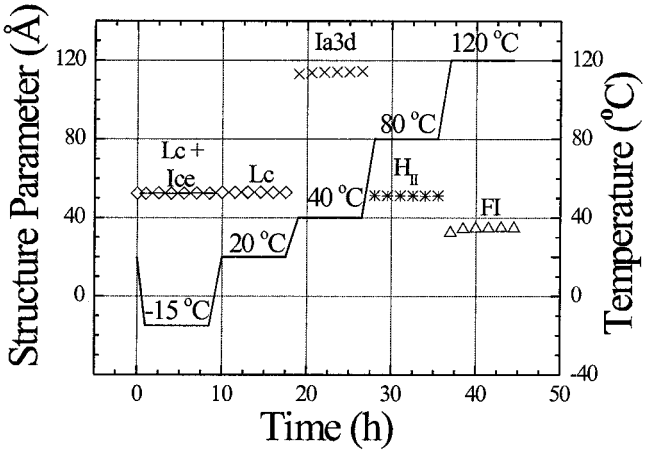

FIGURE 5 Temperature profile and structure parameter relaxation with time for an MNd sample containing 40.1% (w/w) water. The temperature profile is shown as a solid line. Phase identity is as follows: (-) ice, (◇) Lc (d_{001}), (×) cubic-Ia3d (d_{100}), (✳) H_{II} (d_{100}), (Δ) FI.

individual data points. However, to locate phase boundaries with greater accuracy, TRXRD and DSC measurements were made on samples of fixed composition where the properties of the sample were recorded continuously in temperature (see Materials and Methods). Such data are represented as vertical lines in Fig. 4. Those at 11%, 25%, and 35% (w/w) water correspond to data from DSC scans whereas the data at 70% (w/w) water were obtained from a combination of DSC and TRXRD. Thus, Fig. 4 *A* shows the actual phases identified by diffraction and PLM measurements. Phase boundaries, positioned using static and time-resolved diffraction, PLM, and DSC, are shown in Fig. 4 *B*. The excess water boundaries were located using data for phase structure parameter dependence on sample water content of the type shown in Fig. 6 *B*. The boundaries have also been drawn to conform to Gibbs phase rule. It is important to appreciate that the boundaries in Fig. 4 represent a best fit by eye to the data and have an associated estimated error of ±2.5°C and ±2.0% (w/w) water. For ease of comparison, the data in Fig. 4 *A* and the interpreted phase diagram in Fig. 4 *B* are combined in Fig. 4 *C*.

The pure phases in the phase diagram of the MNd/water system, as represented in Fig. 4 *B*, include the Lc phase, the Lα phase, the inverted hexagonal (H_{II}) phase, and the two cubic phases of space group Ia3d and Pn3m. At low temperatures and over the entire composition range studied, the Lc phase dominates the phase diagram. It exists as a pure phase below 5% (w/w) water. The Lc phase is in coexistence with ice below 0°C and with water between 0°C and 13°C. The reason for placing the excess water boundary of the Lc phase at ~5% (w/w) water comes from the fact that ice diffraction is seen in samples with hydration levels above this value but not below it, as discussed in Qiu and Caffrey (1998). The pure Lc phase persists in the dry lipid up to 35°C at which point it begins to melt. It is completely liquid above

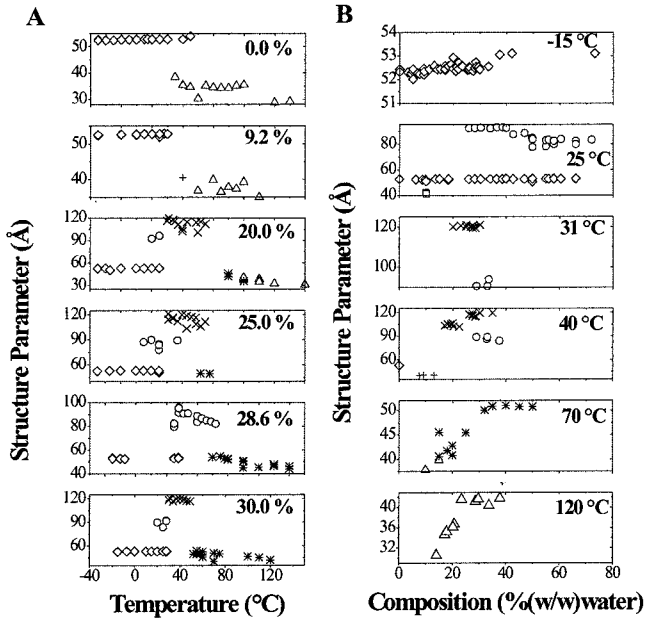

FIGURE 6 Temperature (*A*) and composition (*B*) dependence of the structure parameters of the phases found in the MNd/water system under equilibrium conditions at the indicated sample compositions and temperatures. The identity of each of the phases is as follows: −, ice; ◇, Lc (d_{001}); +, Lα (d_{001}); ×, cubic-Ia3d (d_{100}); ○, cubic-Pn3m (d_{100}); △, FI; (✳), H_{II} (d_{100}). The structure parameter values reported are accurate to ±0.2 Å for the Lc, Lα, and H_{II} phases and ±2.5 Å for the FI, cubic-Ia3d, and cubic-Pn3m phases.

45°C. The pure Lα phase occupies a small, central, triangular region in the phase diagram extending from 6% to 17% (w/w) water and from 29°C to a maximum temperature of 52°C at ~11% (w/w) water. In contrast, the pure cubic-Ia3d phase covers a relatively large area of the diagram. It appears above 26°C and in the range from 15% to 28% (w/w) water and is no longer stable above 65°C. With increasing hydration, the cubic-Ia3d phase gives way to the cubic-Pn3m phase, which remains stable in the 27–56°C range. The composition range in which a pure form of the cubic-Pn3m phase exists is not known. It is likely to be very narrow given the insensitivity of its lattice parameter to hydration (Fig. 6 *B*). This same behavior has been seen for related monoacylglycerols (Briggs, 1994; Briggs and Caffrey, 1994a,b; Briggs et al., 1996; Qiu and Caffrey, 1999, 2000). The pure H_{II} phase emerges at a minimum temperature of 56°C and in the range from 17% to 30% (w/w) water. Its high-temperature limit rises with increasing hydration reaching a maximum of 111°C. At compositions above 30% (w/w) water, it exists in equilibrium with excess water. The FI phase represents the high-temperature phase regardless of composition. The pure FI forms at 45°C in dry MNd. It has a low-temperature limit of 35°C at 4% (w/w) water, which rises with water content to reach a hydration-independent value above 27% (w/w) water at 113.5°C.

Structure parameter temperature and composition dependence

Fig. 6 shows the dependence of the structure parameter on temperature and composition for each of the solid, mesophase, and liquid phases seen in the MNd/water system. The term structure parameter includes the lattice parameter in the ordered phases and the characteristic scattering length associated with the fluid isotropic phase. The general trend is for the structure parameter of the liquid crystalline phases to decrease with increasing temperature (Fig. 6 *A*). The Lc phase lattice dimension is essentially temperature insensitive in the range studied as is expected for the solid state. For pure liquid crystalline phases, the lattice parameter rises with increasing hydration (Fig. 6 *B*). This behavior is typical of the different phases observed in lipid/water systems (Qiu, 1998; Qiu and Caffrey, 1998, 1999, 2000).

Metastable phase diagram

The liquid crystal phases are known to undercool in the same way that water remains liquid at temperatures below 0°C when cooled appropriately (Qiu and Caffrey, 2000). This was observed with the MNd/water system when samples, prepared at room temperature, were first heated to 30°C and then cooled in a slow and stepwise manner. The corresponding phase diagram, which incorporates metastable liquid crystal phases, is shown in Fig. 7 *B*. The most notable difference between the equilibrium (Fig. 7 *A*) and the metastable phase diagram (Fig. 7 *B*) is the existence of the pure cubic-Pn3m phase down to 15°C in the latter. Thus, in the temperature range from 27°C, which is the low-temperature limit of the cubic-Pn3m phase under equilibrium conditions, to 15°C, this mesophase is metastable. This corresponds well with the behavior of previously studied monoacylglycerol/water systems (Qiu, 1998; Qiu and Caffrey, 1998, 1999, 2000).

Calorimetry

MNd/water samples at 11%, 24%, 35%, and 70% (w/w) water were subjected to DSC measurements at scanning rates of 5°C, 10°C, 20°C, 30°C, and 60°C/h. Data was collected in the temperature range from −15°C to 120°C, and transition temperatures and enthalpy changes were corrected for heating rate effects. Sample purity after the calorimetry measurements was examined by TLC. No decomposition was found.

The various phase transitions observed by DSC corresponded within 1–2°C to those identified by x-ray diffraction (Fig. 8). At a composition of 70% (w/w) water, for example, the calorimetric transition onset (To) and completion (Tc) temperatures for the (Lc + Aq)-to-(Pn3m + Aq) transition were 18.3°C and 27.2°C, respectively. These can be compared with 28.2°C, which marks

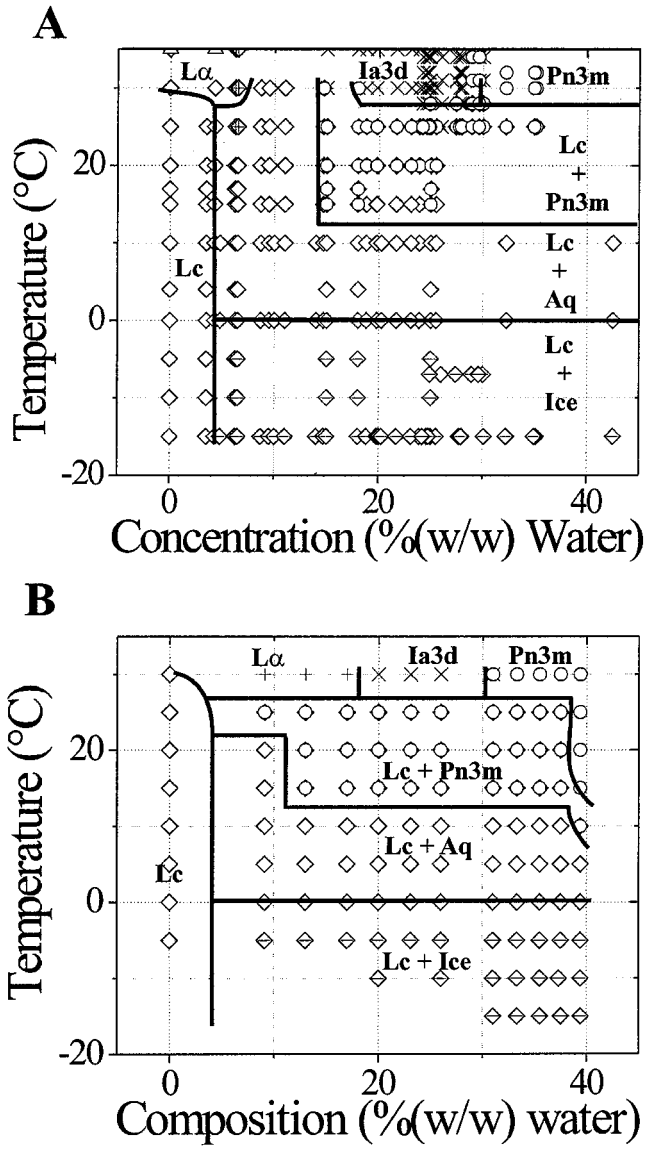

FIGURE 7 Comparison of the low-temperature region of the equilibrium (*A*) and metastable (*B*) phase diagrams of the MNd/water system. Data for *A* were collected in the heating direction and are taken from Fig. 4 *C*. Data for *B* were collected in the cooling direction after the sample was heated initially to 30°C. The identity of the phases is as follows: −, ice; ◇, Lc; +, Lα; ×, cubic-Ia3d; ○, cubic-Pn3m.

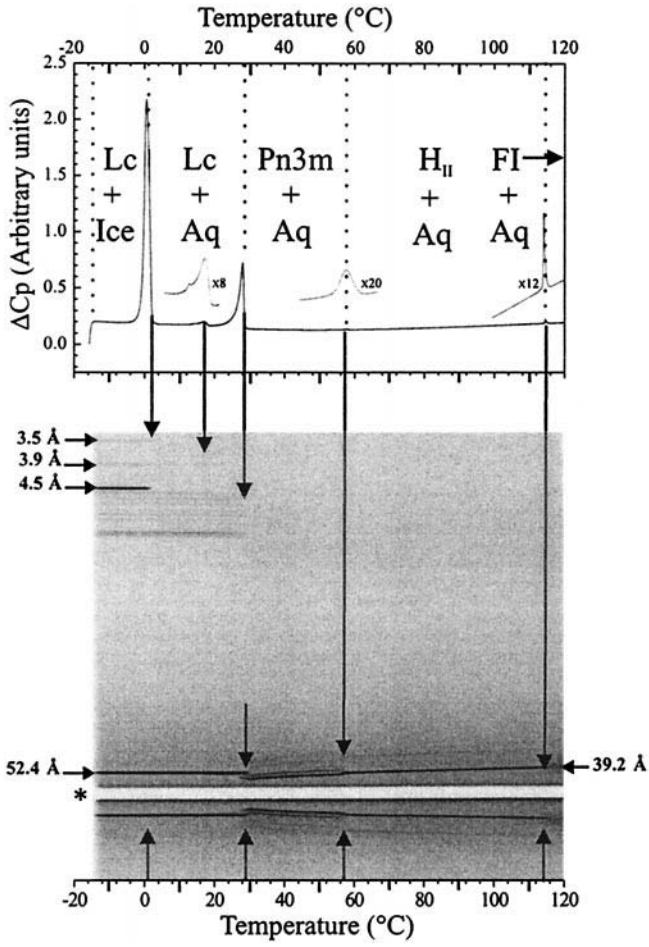

FIGURE 8 Comparison of a calorimetric (*top*) and a TRXRD (*bottom*) measurement on MNd at 70% (w/w) water. Data were collected in the heating direction from −15°C to 120°C at 5°C/h. Phases and phase transitions are identified in the calorimetric trace, whereas the d-spacing of key reflections are included in the TRXRD streak image. The asterisk marks the position of the beam stop. The peak in the calorimetric trace at 19°C represents a polymorphic transition within the Lc phase as indicated by the change in the sharp wide-angle reflections at that temperature. Three of the ice reflections in the wide-angle region of the streak pattern are labeled.

the end of the same transition observed by TRXRD at the same composition. To and Tc for the (Pn3m + Aq)-to-(H_{II} + Aq) phase transition at this same composition are 55.6°C and 57.5°C, respectively. The corresponding transition occurred at 56.5°C when examined by TRXRD. The (H_{II} + Aq)-to-(FI + Aq) transition temperature observed by DSC and TRXRD was 115°C and 115.5°C, respectively.

The enthalpy change for each phase transition has been measured as described in Materials and Methods. In the composition range studied, the (Lc + Aq)-to-(Pn3m + Aq) transition had an enthalpy change of 7.9 ± 0.6 kcal/mol lipid. The corresponding values for the (Pn3m + Aq)-to-(H_{II} + Aq) and the (H_{II} + Aq)-to-(FI + Aq) transitions were 0.1 kcal/mol and ~70 cal/mol, respectively.

Polarized light microscopy

PLM was used to further characterize the phase properties of the MNd/water system and to assist in the identification of the Lα phase, as noted. The Lα phase exhibits several characteristic optical textures when thin samples are viewed between crossed polarizing lenses under a microscope with transmitted light (Gray and Goodby, 1984;

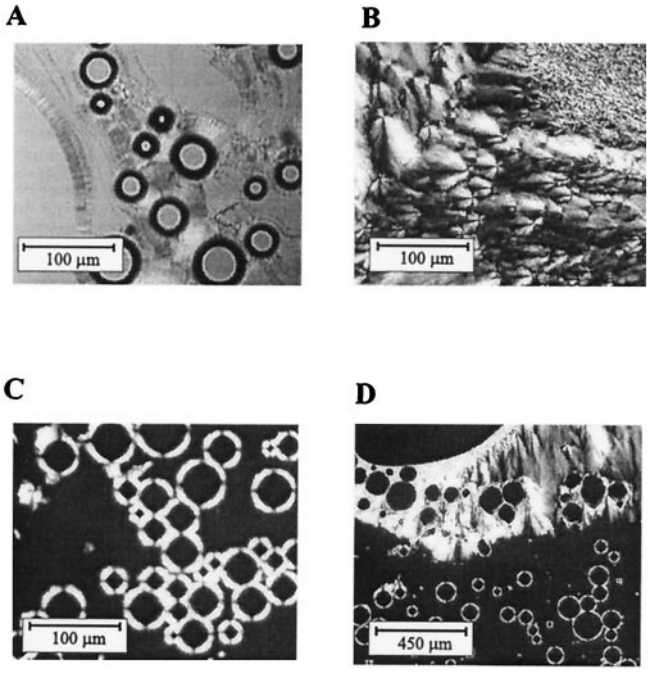

FIGURE 9 Polarized light microscopy images of the MNd/water system. (*A*) Oily streak texture of the Lα phase at 13% (w/w) water and 33°C. The background appears colored due to some anisotropy in the heating cell. (*B*) A coexistence of the Lc and Lα phases in a 13% (w/w) water sample at 24.7°C. The Lc phase is in the upper right hand corner, whereas the Lα region shows the fan-like texture as well as some extinction crosses. (*C*) The extinction-crosses texture of the Lα phase seen in an MNd/water sample at 15% (w/w) water and 35°C. (*D*) A multiphase sample showing the Lc phase in the upper left hand area of the figure and the Lα in two characteristic textures: fan-like in the upper portion of the figure and extinction crosses in the lower portion. This was in a 10% (w/w) water composition sample at 24.7°C.

Rosevear, 1968, 1954). These include the so-called extinction-crosses and oily-streak textures, both of which were seen with MNd under suitable conditions of temperature and hydration (Fig. 9, http://www.lipidat.chemistry.ohio-state.edu/PLMWebsite/PLMPage.html). This result was taken as proof of the existence of the Lα phase in regions of the phase diagram where the corresponding low-angle diffraction pattern consisted of a single ring. The Lc phase was also positively identified in this study. The FI and cubic phases appeared dark and featureless when examined by PLM, reflecting their isotropic and, thus, non-birefringent natures.

DISCUSSION

Equilibrium phase behavior

For comparisons of phase behavior to be valid, it is important that equilibrium conditions be used in obtaining the original data. Accordingly, great care was taken to ensure that the MNd/water phase diagram was constructed with the system at equilibrium and avoiding the commonly encountered non-equilibrium behavior characterized by undercooling. This was achieved in the current study by pre-incubating all samples at −15°C for at least 3 h before any diffraction or calorimetric measurements were made in the heating direction. Following this protocol, all samples were found to be in the Lc phase. The latter is assumed to represent the equilibrium state at low temperature.

Certain samples used to construct the MNd/water phase diagram presented a problem as far as phase identification was concerned in that the corresponding x-ray diffraction patterns contained a single strong and sharp low-angle reflection. An isolated reflection cannot be indexed. However, phase identity was subsequently established as being of the Lα type primarily by PLM but also by a process of eliminating other possible phases based on diffraction behavior and by comparison with the known properties of acyl chain homologs as described previously (Qiu and Caffrey, 1999). Water penetration scans were used to show that the range of phases present in the MNd/water system included the Lc, Lα, H_{II}, and various isotropic phases, as described in Results. Further, a sample at 11% (w/w) water was examined by PLM in the heating direction and was shown to pass from the Lc to the Lα phase at 28.5°C and from the Lα into an optically isotropic phase at 35.4°C (Fig. 4 *A*). The signature oily-streak and extinction-cross textures served to identify the Lα phase (Fig. 9) (Rosevear, 1968, 1954).

The lamellar repeat for the Lα phase was obtained based on the assumption that the single low-angle powder ring in the diffraction pattern corresponded to the basal or (001) reflection. At 40°C and 10% (w/w) water, the d(001) for the Lα phase in MNd was 40.6 Å. The corresponding value for MOl (18:1c9) was 39.0 Å (12.1% (w/w) water; 42.1°C), and for MEc (20:1c11) 39.9 Å (11.5% (w/w) water; 40.0°C) at comparable temperatures and compositions. The similarity of the lattice parameter values for the three acyl chain homologs lends credence to the Lα phase assignment in the case of the MNd system.

Comparison of the equilibrium and metastable phase diagrams

Metastability of the liquid crystal phases is a hallmark of the monoacylglycerols (Briggs and Caffrey, 1994b; Qiu and Caffrey, 1998, 1999, 2000). It comes about when samples, prepared at room temperature, are cooled quickly to low temperatures. We have found that undercooling of the Lα and cubic phases can persist to sub-0°C temperatures. However, incubating the sample at −15°C for several hours usually resets the system into the equilibrium Lc or solid phase. This is what we found in the case of the MNd/water system also.

A comparison of the MNd/water (partial) phase diagrams collected under equilibrium and metastable conditions is shown in Fig. 7. They are remarkably similar, indicating

that the tendency to undercool is not pronounced for this particular lipid. This is likely due to the existence of the Lc phase at room temperature over the entire hydration range. The major difference between the equilibrium and metastable diagrams is observed in the high-water-content region where the cubic-Pn3m phase persists to considerably lower temperatures under metastable conditions. Thus, the equilibrium diagram has the pure cubic-Pn3m phase in isolation existing down to 27°C. The corresponding temperature under metastable conditions is ~15°C. Undercooling of the cubic phase is expected behavior (Briggs and Caffrey, 1994b; Qiu and Caffrey, 1998, 1999, 2000).

Although the extent of undercooling is not particularly great, it might still be exploited in situations where the cubic phase is required of a monoacylglycerol with MNd's physico-chemical properties to temperatures down to 15°C. This issue, applied to the crystallization of membrane proteins in lipidic mesophases, has been addressed separately (Caffrey, 2000).

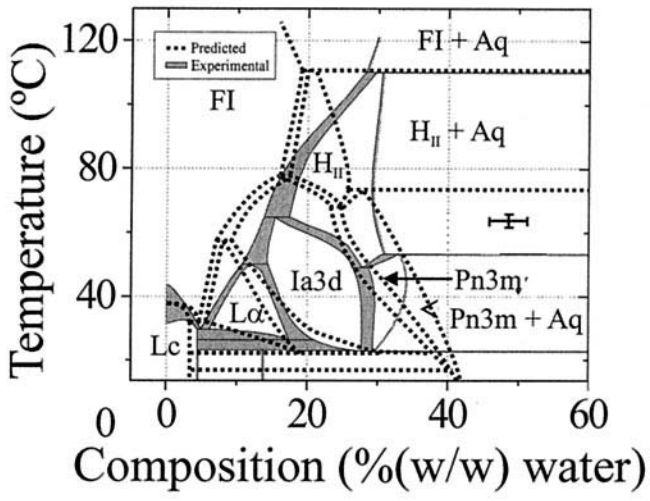

FIGURE 10 A comparison of the predicted (*dotted lines*) and experimentally determined (*shaded boundaries*) phase diagram of the MNd/water system. Some of the two-phase boundaries in the experimental diagram were widened to make them more visible. The error bars shown indicate the error associated with the placement of the phase boundaries in both the predicted and experimental phase diagrams. The predicted and experimental phase diagrams were taken from Figs. 3 and 4B, respectively.

Comparison of the predicted and experimental phase diagrams

Before embarking on a quantitative comparison of the predicted and experimentally determined phase diagrams for the MNd/water system, it is important to recognize the magnitude of the uncertainties or errors associated with each. The experimental phase diagram shown in Fig. 4 *B* is based primarily on data collected at discrete values of temperature and composition in increments of generally 2–5°C and 2–5% (w/w) water (except at concentrations above 35% (w/w) water, for reasons already discussed), respectively (Fig. 4 *A*). Phase boundaries were fit to these data by eye and have an estimated error of ±2.5°C and ±2.0% (w/w) water.

The level of uncertainty in the case of the predicted phase diagram is somewhat greater than that just described for the experimental diagram. In the first place, the predicted diagram is itself based on experimentally determined phase diagrams each of which has the aforementioned boundary position errors. Second, the predicted transition temperatures and compositions were obtained from experimental data on two, or at most three, other systems (see Fig. 1, *C–F*). Further, the assumption made in all predictions is that transition temperature and composition depend linearly on acyl chain tail (*T*) and neck (*N*) length. Thus, with just two or three data points upon which to base a prediction by interpolation or extrapolation, the corresponding predicted values can really be taken only as approximations with sizable associated errors. This is the situation represented in Fig. 3. Note also that the phase diagram in Fig. 3 was itself drawn based on a very few data points (asterisks and circles in Fig. 3) and on the behavior observed with related MNd homologs (Briggs, 1994; Briggs and Caffrey, 1994a,b; Briggs et al., 1996; Qiu, 1998; Qiu and Caffrey, 1998, 1999, 2000). In light of these assorted issues, we consider the assigned estimated errors of ±5.0°C and ±5.0% (w/w) water for the predicted phase diagram in Figs. 3 and 10 to be conservative.

To facilitate the comparison, Fig. 10 shows an overlay of the experimental (shaded boundaries) and predicted (dotted lines) phase diagrams for the MNd/water system in the range 15–120°C and 0–60% (w/w) water. We have chosen not to examine the phase behavior at low temperatures where the Lc phase dominates because it is the liquid crystal phases, and not the solid state, that are the focus of attention in this study. The relative areas of the pure phases in the two diagrams have been measured and are reported in Table 1.

A perusal of the data in Fig. 10 shows that the predicted phases are all present in the experimental system and that they are there in the expected relative positions with respect to temperature and composition. Thus, the Lα, cubic-Ia3d, cubic-Pn3m, H_{II}, and FI phase regions in the predicted and experimental diagrams overlap remarkably well considering the phase boundary errors noted. There are three regions where the two diagrams are at variance, however. These include the lower temperature limit of the H_{II} phase, the upper hydration range of the cubic-Ia3d phase, and the upper hydration boundary of the pure FI phase. The upper hydration boundary of the pure FI phase is shifted to lower water contents in the case of the predicted diagram. The lower temperature limit of the H_{II} phase has a predicted transition temperature ~20°C higher than is observed experimentally. Further, the cubic-Ia3d region extends to con-

TABLE 1 Relative areas occupied by the phases and phase coexistence regions in the predicted and experimental phase diagrams for the MNd/water system

	Area (%)	
Phase identity	Experimental	Predicted
FI	25	19
H_{II} + Aq	23	19
Cubic-Pn3m + Aq	14	19
FI + Aq	8	12
H_{II}	7	3
Cubic-Ia3d	6	12
Lc + Cubic-Pn3m	5	7
Lα	4	4
Lc	2	2
Cubic-Pn3m	2	4
Total	96	100

Area was quantified based on an analysis of Fig. 10 using CorelDRAW 9 (Corel Corp., Ottawa, ON, Canada). Area is expressed as a percentage of the total area, where 100% corresponds to the area defined by the temperature and composition ranges from 0°C to 120°C and 0 to 60% (w/w) water, respectively.

centrations ~10% (w/w) water higher than that of the experimental data. The latter comparison is based on a predicted value obtained by using just two data points (Fig. 1 *D*). We bring these differences to the reader's attention but choose not to proffer an explanation given the uncertainties already discussed.

Overall, the predicted and experimentally determined phase diagrams agree quite well. The major limitation is the size of the database of experimental phase diagrams upon which the predictions are made. The current work contributes to making good this deficit in that a new experimental phase diagram, that of the MNd/water system, has been constructed. As the database grows, so too will our ability to predict the lyotropic and thermotropic properties of the monoacylglycerol/water and related systems with improved accuracy and resolution.

CONCLUSIONS

In this study, we set out to test the predictive power of a somewhat limited database of temperature-composition phase diagrams for a monoacylglycerol/water system series. The intent was to use the existing phase diagrams to predict the phase behavior of an acyl chain homolog, MNd (19:1c10). The prediction was based on the assumption that thermotropic and lyotropic phase behavior changes linearly with chain length. Further, no regard was paid to double bond position along the chain or to a possible odd-even chain length alternation in phase behavior (Boese et al., 1999). The sense was that the accuracy of the prediction was not sufficiently good to be sensitive to these effects, which, at this stage, we consider to be of second order.

The predicted MNd/water phase diagram was based on previously established equilibrium phase behavior of the MOl (18:1c9), MEc (20:1c11), MEr (22:1c13), MHt (17:1c10), and MPt (15:1c10)/water systems. The corresponding equilibrium phase diagram for the chosen system was constructed using a variety of experimental methods. To within the uncertainties of the prediction, which are quite considerable as discussed, the experimental and the predicted phase diagrams agreed remarkably well.

This exercise illustrates the power of the predictive method and points to its utility in describing the phase behavior of systems for which phase diagrams are not available or cannot be obtained, for whatever reason. However, the exercise also serves to highlight current shortcomings in the approach, the most serious of which is the paucity of entries in the database of experimental phase diagrams. The reliability and accuracy of the predictions will obviously grow as more phase diagrams are generated and the principles that link molecular structure to mesophase behavior are elucidated.

The benefits of this approach are considerable, especially in the area of rational design. Thus, for example, a very specific phase behavior may be called for in a certain medical, industrial, or experimental application. Using the principles noted above, it should be possible to choose rationally a particular lipid species (or mixture of lipids and other components) that will provide such properties. It is then a matter of obtaining the lipid commercially, from a natural source, or by synthesis.

In the current work, the focus has been on mesophase behavior. Equally important but not discussed in any detail here is the issue of phase microstructure. This refers to how space is divided between the lipidic and aqueous compartments within the bulk mesophases. Microstructure can profoundly influence the suitability of a given lipid for a particular application and is an integral part of the rational design approach. Where possible, microstructure as well as phase behavior information should be collected together, as was done in the current study. An evaluation of the microstructure characteristics of the MNd/water system will be presented elsewhere.

We thank the members of our research group for invaluable input on this work. They include X. Ai, V. Cherezov, J. Clogston, H. Qiu, and D. Siegel. Relevant data reported in this paper have been deposited in the Lipid Data Bank (http://www.ldb.chemistry.ohio-state.edu).

This work was funded in part by the National Institutes of Health (GM56969 and GM61070) and the National Science Foundation (DIR9016683 and DBI9981990).

REFERENCES

Blanton, T. N., T. C. Huang, H. Toraya, C. R. Hubbard, S. B. Robie, D. Louer, H. E. Gobel, G. Will, R. Gilles, and T. Raftery. 1995. JCPDS-International Centre for diffraction data round robin study of silver

behenate: a possible low-angle x-ray diffraction calibration standard. *Powder Diffract.* 10:91–95.

Boese, R., H-C. Weiss, and D. Blaser. 1999. The melting point alternation in the short-chain *n*-alkanes: single-crystal x-ray analyses of propane at 30 K and of *n*-butane to *n*-nonane at 90 K. *Angew. Chem. Int. Ed.* 38:988–992.

Boulikas, T. 1996. Liposome DNA delivery and uptake by cells. *Oncol. Rep.* 3:989–995.

Briggs, J. 1994. The phase behavior of hydrated monoacylglycerols and the design of an x-ray compatible scanning calorimeter. Ph.D. Thesis. The Ohio State University, Columbus, OH.

Briggs, J., and M. Caffrey. 1994a. The temperature-composition phase diagram and mesophase structure characterization of monopentadecenoin in water. *Biophys. J.* 67:1594–1602.

Briggs, J., and M. Caffrey. 1994b. The temperature-composition phase diagram of monomyristolein in water: equilibrium and metastability aspects. *Biophys. J.* 66:573–587.

Briggs, J., H. Chung, and M. Caffrey. 1996. The temperature-composition phase diagram and mesophase structure characterization of the monoolein/water system. *J. Phys. II France.* 6:723–751.

Brown, D. A., and E. London. 1998. Functions of lipid rafts in biological membranes. *Annu. Rev. Cell Dev. Biol.* 14:111–136.

Brown, D. A., and E. London. 2000. Structure and function of sphingolipid- and cholesterol-rich membrane rafts. *J. Biol. Chem.* 275: 17221–17224.

Caffrey, M. 1989. A lyotropic gradient method for liquid crystal temperature-composition-mesomorph diagram construction using time-resolved x-ray diffraction. *Biophys. J.* 55:47–52.

Caffrey, M. 2000. A lipid's eye view of membrane protein crystallization in mesophases. *Curr. Opin. Struct. Biol.* 10:486–497.

Cheng, A., B. Hummel, H. Qiu, and M. Caffrey. 1998. A simple mechanical mixer for small viscous samples. *Chem. Phys. Lipids.* 95:11–21.

Chung, H., and M. Caffrey. 1995. Polymorphism, mesomorphism, and metastability of monoelaidin in excess water. *Biophys. J.* 69:1951–1963.

Engström, S. 1990. Cubic phases as drug delivery systems. *Polymer Prep.* 31:157–158.

Gray, G. W., and J. W. G. Goodby. 1984. Smectic liquid crystals. Leonard Hill, Glasgow, UK.

Jones, M. N., and D. Chapman. 1995. Micelles, monolayers, and biomembranes. John Wiley and Sons, New York.

Landau, E. M., G. Rummel, S. W. Cowan-Jacob, and J. P. Rosenbusch. 1997. Crystallization of a polar protein and small molecules from the aqueous compartment of lipidic cubic phases. *J. Phys. Chem. B.* 101: 1935–1937.

Lasic, D. D. 1997. Recent developments in medical applications of liposomes: sterically stabilized liposomes in cancer therapy and gene delivery in vivo. *J. Control. Release.* 48:203–222.

Luecke, H., H. T. Richter, and J. K. Lanyi. 1998. Proton transfer pathway in bacteriorhodopsin at 2.3 angstrom resolution. *Science*. 280: 1934–1937.

Rosevear, F. B. 1954. The microscopy of the liquid crystalline neat and middle phases of soaps and synthetic detergents. *J. Am. Oil Chem. Soc.* 31:628–639.

Rosevear, F. B. 1968. Liquid crystals: the mesomorphic phases of surfactant compositions. *J. Soc. Cosmetic Chemists.* 19:581–594.

Qiu, H. 1998. The mesophase behavior of the monoacylglycerol/water systems: application in drug delivery. Ph.D. Thesis. The Ohio State University, Columbus, OH.

Qiu, H., and M. Caffrey. 1998. Lyotropic and thermotropic phase behavior of hydrated monoacylglycerols: structure characterization of monovaccenin. *J. Phys. Chem. B.* 102:4819–4829.

Qiu, H., and M. Caffrey. 1999. Phase behavior of the monoerucin/water system. *Chem. Phys. Lipids.* 100:55–79.

Qiu, H., and M. Caffrey. 2000. Phase properties of the monoolein/water system: metastability and equilibrium aspects. *Biomaterials.* 21: 223–234.

Simons, K., and E. Ikonen. 2000. How cells handle cholesterol. *Science.* 290:1721–1726.

Weast, R. C., and M. J. Astle. 1982. Handbook of Chemistry and Physics. CRC Press, Boca Raton, FL.